AERODYNAMIC CHARACTERISTICS OF WING-BODY-COMBINATIONS AT HIGH ANGLES OF ATTACK

D. Hummel, TU Braunschweig*
H. John, W. Staudacher, MBB-München**

Federal Republic of Germany

Abstract

Wind-tunnel investigations have been carried out on a series of wing-body-combinations composed of a fuselage and 9 different wings in high wing and low wing positions. Six-component balance measurements and flow visualizations have been performed up to high angles of attack. The effects of wing planform and of a body on the $c_{l\beta}$-characteristics of the various configurations have been studied in detail. Unstable rolling moments are caused by unsymmetrical vortex breakdown, by unsymmetrical formation of deadwater regions and by different flow structures on both sides of the wing. Configurations with a high wing position are much more unstable than those with a low wing position. By means of small modifications of the body contour favourable interference effects could be created which led to stable rolling moments in the whole angle of attack range.

1. Introduction

For modern aerodynamic concepts like hybrid wings and delta-canard configurations high angle of attack manœuvers are featured by the existence of strong vortical flows which are governed by the following phenomena:

In symmetrical flow already at small angles of attack the flow separates from the wing leading-edges and from the body. Concentrated vortices are formed over the upper surface of the configuration and interference of the body vortices with the wing vortices is observed, depending on the actual shape of the configuration. At high angles of attack vortex breakdown occurs in the wing vortices. The breakdown position crosses the wing trailing-edge at a certain angle of attack, depending on the wing aspect ratio, and moves upstream with increasing angle of attack. The maximum lift coefficient is reached when the pressure increase on the lower side is compensated by the decrease of suction on the upper side of the configuration; see e.g. D. Hummel [1]. For moderate aspect ratio wings the corresponding flow on the upper surface shows almost completely destroyed vortices and in most parts of the configuration an unsteady separated flow of deadwater type is present.

In unsymmetrical flow the lift of the windward half of the configuration is larger than that of the leeward half, which leads to stable rolling moments (lateral stability $c_{l\beta} < 0$). This is true for attached flow, for separated flow with concentrated vortices without vortex breakdown as well as for the flow at moderate angles of attack with vortex breakdown over the windward side of the configuration. At very high angles of attack, however, especially in the neighbourhood of the maximum lift coefficient and in the post-stall regime, lateral stability is considerably reduced and even unstable rolling moments may occur. This unfavourable behaviour has been found for a large number of configurations as for instance by D. Hummel, G. Redeker [2], W. Kraus, H. John [3,4], W. Staudacher, B. Laschka, Ph. Poisson-Quinton, J.P. Ledy [5], C.W. Smith, C.A. Anderson [6], J.E. Lamar, J.M. Luckring [7], A.M. Skow, A. Titiriga, W.A. Moore [8]. From these investigations unstable rolling moments at high angles of attack seem to be a typical characteristic of moderate aspect ratio wing-body-combinations. Thus, for such configurations the maximum useable lift is limited by lateral/directional problems which keep them away from their full lift potential. Well known criteria such as LCDP (Lateral Control Departure Parameter) and the $c_{n\beta\,dyn}$-parameter are helpful in defining the problem areas. The parameter

$$c_{n\beta\,dyn} = c_{n\beta} \cdot \cos\alpha - \frac{I_z}{I_x} \cdot c_{l\beta} \cdot \sin\alpha$$

depends on the ratio of the inertia moments I_z/I_x and for stable flight $c_{n\beta\,dyn} > 0$ is necessary. For slender, highly swept configurations having a high ratio of I_z/I_x the derivative $c_{l\beta}$ becomes very important and a divergence of this derivative at high angles of attack leads to serious problems.

In the last years this divergence problem has been analysed experimentally within a close cooperation between the Institut für Strömungsmechanik at Technische Universität Braunschweig and Messerschmitt-Bölkow-Blohm GmbH in Ottobrunn. In this program a typical wing-body-combination has been chosen in order to analyse the lateral instability and to understand the physics of the flow which leads to this phenomenon. Starting from a basic configuration the wing planform has been varied systematically in order to investigate the planform effects on lateral stability. Recently it has been shown that lateral stability may be influenced by modifications of the leading-edges of the wing: D. Welte, S. Ehekircher [9] investigated

* Prof. Dr.-Ing. D. Hummel, Institut für Strömungsmechanik, Technische Universität Braunschweig.
** Dr.-Ing. H. John, Dipl.-Ing. W. Staudacher, Messerschmitt-Bölkow-Blohm GmbH, München.

some unusual control surfaces, W. Kraus [10] modified the leading-edge shape by means of nose flaps and W. Staudacher [11] has demonstrated that double-hinged leading-edge flaps completely eliminated the $c_{l\beta}$-problem found on a cropped delta wing configuration. Although some investigations of this kind have been performed within the present experimental program, wing modifications other than planform variations are not included in this report. On the other hand some minor modifications of the shape of the fuselage led to considerable improvements in lateral stability. These results are included in the subsequent report on the program.

2. Notations (see Figs. 1 and 15)

$A = b^2/S$	Aspect ratio
$D = 2R$	Body diameter
$L = L_F+L_C+L_R$	Body total length
L_C	Length of cylindrical part of the body
L_F	Length of front part of the body
L_R	Length of rear part of the body
R	Body maximum radius
$Re = U_\infty \cdot L/\nu$	Reynolds Number
S	Wing area (LE and TE within the body extended to the axis y=0)
U_∞	Free stream velocity
b	Span
$c(y)$	Local chord
$c_R = c(R)$	Root chord of wing-body-combination
$c_r = c(0)$	Root chord of wing alone
$c_t = c(s)$	Tip chord
$c_\mu = \frac{1}{S}\int_{-s}^{+s} c^2(y)dy$	Reference chord
c_L, c_D, c_Y	Coefficients for lift, drag and side-force, based on S
c_m, c_l, c_n	Coefficients for pitching moment (based on S and c_μ), rolling moment and yawing moment (based on S and s) about body-fixed axes through N_{25}*, signs according to Fig. 1
$c_{l\beta} = \left(\frac{\partial c_l}{\partial \beta}\right)_{\beta=0}$	Lateral stability
$c_{n\beta} = \left(\frac{\partial c_n}{\partial \beta}\right)_{\beta=0}$	Directional stability
e	Distance between body apex and wing geometric neutral point N_{25}
h	Height of body fence
l	Length of body fence
s	Half span
t	Wing thickness
x,y,z	Wing-fixed coordinates, origin at wing apex
x'_{N25}	Distance of wing geometric neutral point N_{25} from the rear end of the wing at y=0 ($e + x'_{N25} = L_F + L_C$)
z_{N25}	Distance of wing geometric neutral point N_{25} (at t/2) from the body axis (>0 for high wing, <0 for low wing)
Λ	Angle of sweep
α	Angle of attack (in plane y=0)
β	Angle of sideslip
$\lambda = c_t/c_r$	Taper ratio
φ	Fence position (Fig. 15)

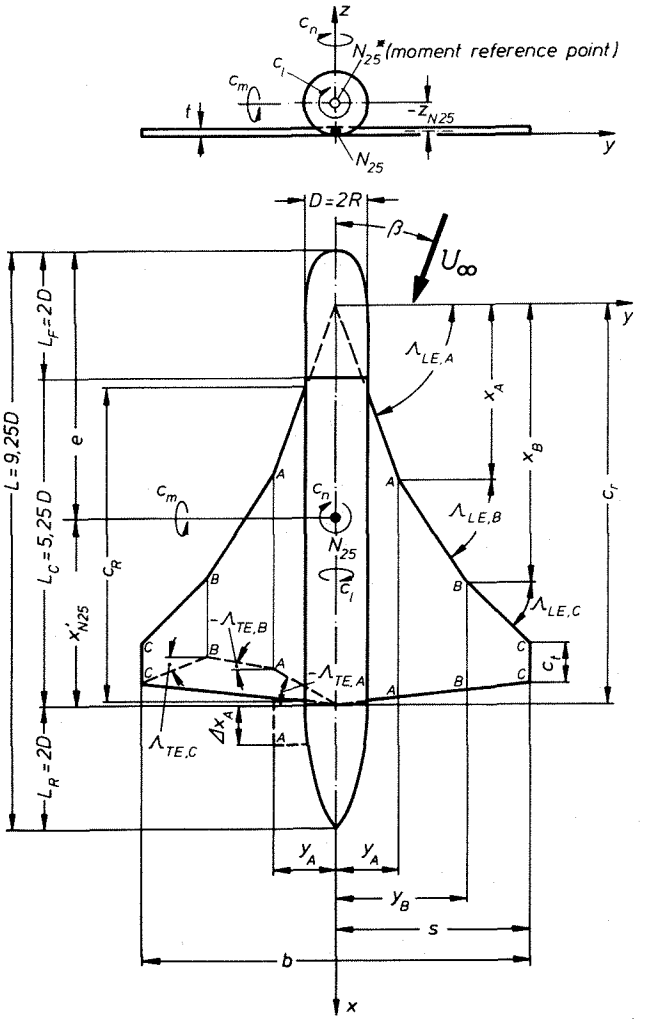

Fig. 1: Notations

Subscripts

LE	Leading-edge
TE	Trailing-edge
A,B,C	Quantities belonging either to the kinks A,B and the wing tip C or to the sections of the wing up to these points

3. Program and experimental set-up

3.1 Program

3.1.1 Approach

The investigations have been carried out on a series of wings and wing-body-combinations. Starting point was a typical configuration which showed the c_{l_β}-divergence quite clearly. The first aim was to understand the physics of this phenomenon for the basic configuration.

It is well known that the c_{l_β}-derivative is very sensitive to small changes of the shape of the configuration. Therefore in a second step some geometric parameters of the configuration have been varied systematically in order to find the basic effects of wing planform shape as well as the body effect. For this purpose the following variations of the geometry have been applied for

(i) Wing planform effects (b=const.)
- Leading-edge sweep } for inboard and
- Trailing-edge sweep } outboard wing
- Position of the kinks in leading-edge and trailing-edge
- Positive and negative strakes

(ii) Body effect
- Wing alone (without body)
- Wing height (low wing, high wing).

The overview on the effects of these variations on the c_{l_β}-derivatives should enable the designer to chose the most favourable configuration.

Furthermore the corresponding understanding of the physics could be used to influence the flow in such a way that even no c_{l_β}-divergence takes place. Therefore it was the third aim of this program to apply "trigger" effects to achieve stable c_{l_β}-derivatives in the whole angle of attack range. For this purpose tests have been carried out on the effects of

(iii) Trigger devices
- Vortex generators
- Body chines (ledges, fences).

The latter turned out to be very effective and results of these investigations will be described subsequently.

3.1.2 Design

From the configurational side some constraints were superimposed for the design of the configurations. These constraints are:

(i) A single fuselage of diameter D should be applied for all wing-body-combinations and the ratio D/b should be kept constant. This means that wings of constant span b have been designed, which leads to similar structures and drag characteristics for all wings.

(ii) The variations in root chord length c_R should be as small as possible in order to avoid extensive modifications of the structure.

Fig. 2 shows an overview of the model matrix derived so far and indicates the main parameters which have been varied. Starting point is the basic configuration (1), which has been tested as wing alone (01) and as wing-body-combination with low wing (L1) and high wing (H1) location.

The configurations (2), (3) and (7) show minor changes of the leading-edge contours near the wing-body intersection in the form of a straight negative, a straight positive and a curved negative strake. For the configurations (8) and (9) the shape of the leading-edge has been kept constant and the trailing-edge has been modified by a so-called "Küchemann"-fairing (8) and by a kinked trailing-edge (9). It may be noted that comparing the configurations (3) and (8) as well as (2), (7) and (9) the aspect ratio A is roughly constant. Within the given constraints higher aspect ratios could only be derived by tailoring the leading-edge and/or trailing-edge contours. For configuration (4) the leading-edge sweeps are the same as for the basic configuration (1), but the leading-edge kink is shifted more inboard and the trailing-edge is also broken at the same spanwise distance. For the configurations (5) and (6) the kink in leading-edge and trailing-edge is shifted even more inboard; the trailing-edge shape is kept constant and the leading-edge is chosen similar to well-known strake-wing configurations.

3.2 Models

The geometric data of the wings are collected in Tab. 1. The corresponding notations may be taken from Fig. 1. For wing (7) the root chord c_R of the wing-body-combination is shortened by 8 % as compared to the basic configuration and the leading-edge starts there at a sweep angle $\Lambda_R = 25^0$. The curved negative strake is designed as a fourth order polynomial, which meets the straight leading-edge of the basic wing (1) at $y_A/s = 0.25 + 0.75\,D/b$ continuously with respect to slope and curvature. The wing (8) is equipped by a so-called "Küchemann"-fairing at the trailing-edge. For this purpose the inner part of the basic wing is extended by $\Delta x_A/s = 0.21$ (see Fig. 1) and the trailing-edge kink is located at $y_A/s = 0.24$. All wings have the same span (b = 500 mm). They are manufactured as thin flat plates with rounded edges, but due to the very small thickness of $t/b = 0.167 \cdot 10^{-2}$ these wings may be regarded as sharp-edged.

The fuselage consists of a cylindrical portion of length $L_C = 5.25\,D$ and attached are front and rear parts of length $L_F = L_R = 2\,D$. Their shapes have been designed as a polynomial of second order plus a square root term and as a fourth order polynomial, which meet the cylindrical part continuously with respect to slope and curvature. The body diameter is D = 80 mm.

The combination of the fuselage with the wings leads to the configurations shown in Fig. 2. Their geometric data are summarized in Tab. 2. The wings

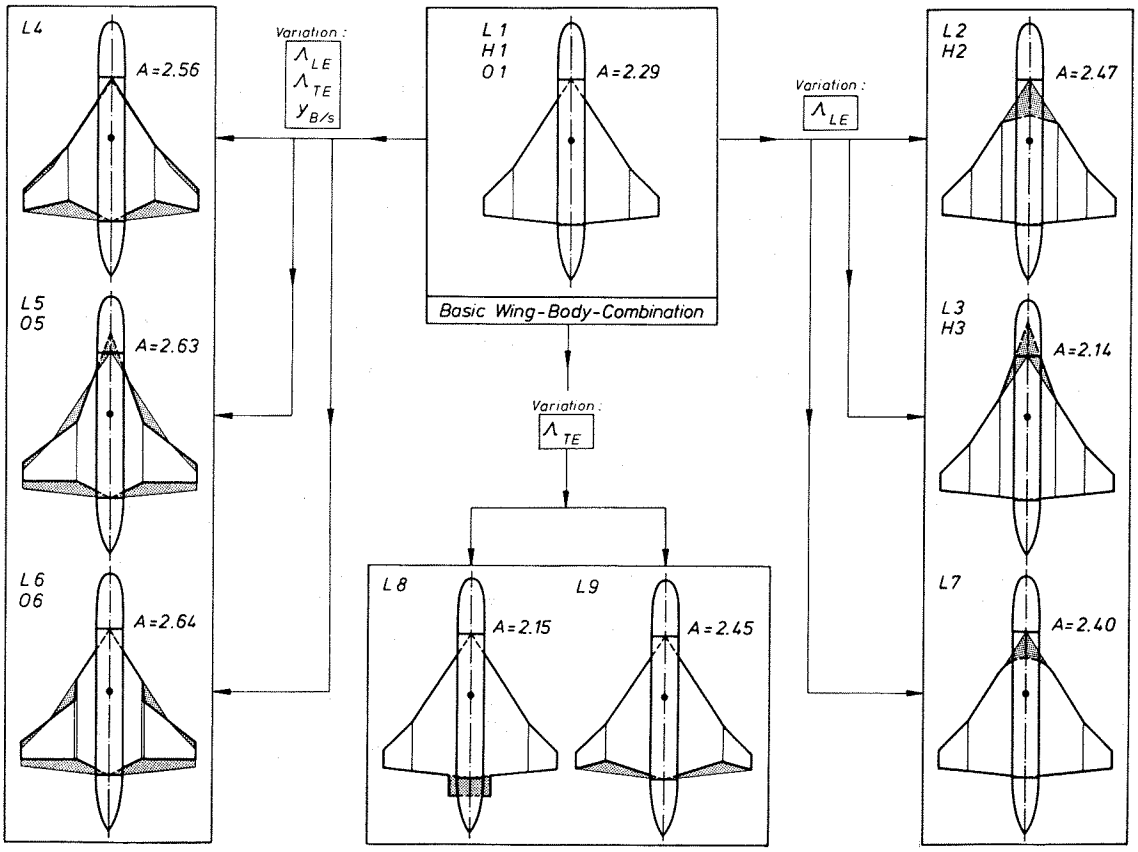

Fig. 2: Model matrix of the wing-body-combinations
L Low wing, H High wing, O Wing alone
▒▒▒ Planform modifications compared to the basic wing (1)

Wing		1	2	3	4	5	6	7	8	9
Aspect ratio	$A = b^2/S$	2.29	2.47	2.14	2.56	2.63	2.64	2.40	2.15	2.45
Taper ratio	$\lambda = l_t/c_r$	0.121	0.160	0.098	0.146	0.105	0.121	0.148	0.107	0.121
Leading-edge sweep	$\Lambda_{LE,A}$	-	15^0	70^0	-	-	57^0	curved	-	-
	$\Lambda_{LE,B}$	57^0	57^0	57^0	57^0	70^0	85^0	57^0	57^0	57^0
	$\Lambda_{LE,C}$	45^0	45^0	45^0	45^0	37.5^0	37.5^0	45^0	45^0	45^0
Trailing-edge sweep	$\Lambda_{TE,A}$	-	-	-	-	-	-26^0	-6^0	-	-
	$\Lambda_{TE,B}$	-6^0	-6^0	-6^0	-26^0	-26^0	0^0	-6^0	-6^0	-18^0
	$\Lambda_{TE,C}$	-6^0	-6^0	-6^0	$+13^0$	0^0	0^0	-6^0	-6^0	$+13^0$
Positions of kinks	y_A/s	-	0.320	0.320	-	-	0.380	(0.28)	-	-
	y_B/s	0.667	0.667	0.667	0.500	0.380	0.400	0.667	0.667	0.667
Position of N_{25}	$x_{N'25}/b$	0.424	0.408	0.481	0.439	0.453	0.441	0.397	0.423	0.441
Reference chord	c_μ/b	0.540	0.480	0.616	0.500	0.515	0.508	0.505	0.606	0.533
Root chord	c_r/b	0.833	0.629	1.026	0.819	0.953	0.830	0.681	0.940	0.833
Thickness	$(t/b) \cdot 10^2$	0.167	0.167	0.167	0.167	0.167	0.167	0.167	0.167	0.167

Tab. 1: Geometric data of the wings

Combination	L1/H1	L2/H2	L3/H3	L4	L5	L6	L7	L8	L9
Relative fuselage width, D/b	0.16	0.16	0.16	0.16	0.16	0.16	0.16	0.16	0.16
Rear position of N_{25}, e/L	0.497	0.508	0.459	0.487	0.477	0.486	0.516	0.516	0.486
Relative wing height, Z_{N25}/D	±0,481	±0.481	±0,481	-0,481	-0,481	-0,481	-0,481	-0,481	-0,481

Tab. 2: Geometric data of the wing-body-combinations

are added to the fuselage in such a way that the rear end of the wing coincides with the rear end of the cylindrical part of the fuselage. Only in the case of wing (8) the "Küchemann"-fairing is located in the rear part of the fuselage. The height of the wings is adjusted in such a way that for a high wing the upper surface of the wing is tangential to the cylindrical contour of the fuselage. The junction between wing and fuselage is filled up to form a 90^0-corner along the whole root chord c_R and upstream and downstream a proper contour is modelled by plasticin.

3.3 Description of the tests

The experimental investigations have been performed in the 1.3 m wind-tunnel of the Institut für Strömungsmechanik of Technische Universität Braunschweig. The free-stream velocity was $U_\infty = 40\,m/s$, which corresponds to a Reynoldsnumber, based on body length, of $Re = 2 \cdot 10^6$.

Six-component measurements have been carried out for

$-6^0 \leqq \alpha \leqq +40^0$ and for $-5^0 \leqq \beta \leqq +15^0$.

In addition the flow on the upper surface of the configurations has been studied by means of oilflow patterns. For this purpose the black model surface was painted by a mixture of aluminiumoxide-powder and petroleum and benzine (ratio of components: 1 g aluminiumoxide : 3 cm^3 petroleum : 1 cm^3 benzine) and exposed to the flow for about half a minute.

For some configurations additional flow visualizations have been carried out in the 33 x 25 cm^2 water-tunnel of the Institut für Strömungsmechanik at Technische Universität Braunschweig. In these investigations the flow has been made visible by means of dye injection into the vortices. The free-stream velocity was $U_\infty = 12\,cm/s$ and the corresponding Reynoldsnumber was $Re = 1.8 \cdot 10^4$.

4. Results

From the various aerodynamic data for each configuration the diagrams $c_L(\alpha)$ and $c_{l\beta}(\alpha)$ are shown subsequently. The diagram $c_L(\alpha)$ indicates the flow situation in symmetrical flow ($\beta = 0$) and the diagram $c_{l\beta}(\alpha)$ is the main result of the present investigations which describes the behaviour of the configurations for deviations ($\beta \neq 0$) from the symmetrical flow situation.

4.1 Planform effects for the basic wing

The aerodynamic characteristics of the basic wing (1) without fuselage (Configuration 01) are shown in Fig. 3.

For $\alpha < 10^0$ a slightly nonlinear lift curve turns out which is due to the formation of concentrated vortices over the upper surface of the wing. In unsymmetrical flow ($\beta \neq 0$) the angles of sweep are reduced on the windward side of the configuration. Correspondingly the vortex on the windward side is strengthened and that on the leeward side is weakened. As in attached flow this effect leads for $\alpha < 10^0$ to higher lift on the windward side as compared to the leeward side and therefore stable (negative) rolling moments are observed.

In symmetrical flow ($\beta = 0$) vortex breakdown crosses the trailing-edge of the wing at $\alpha \approx 10^0$ and for larger angles of attack the lift curve slope is reduced as indicated in Fig. 3. In unsymmetrical flow vortex breakdown moves upstream in the vortex on the windward side and downstream in the vortex on the leeward side. The asymmetry in vortex breakdown leads to additional destabilizing (positive) rolling moments as marked in Fig. 3. The symmetrical flow situation in the region of $c_{L\,max}$ may be taken from Fig. 4a. In both vortices vortex breakdown occurs close to the wing apex. Only a small portion of the vortices shows an ordinary development and the flow over the

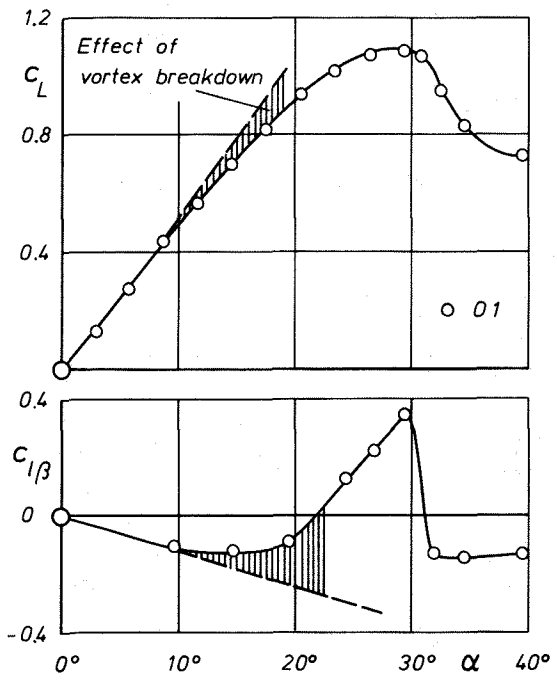

Fig. 3: Aerodynamic characteristics of configuration 01 (Basic wing (1) without fuselage)

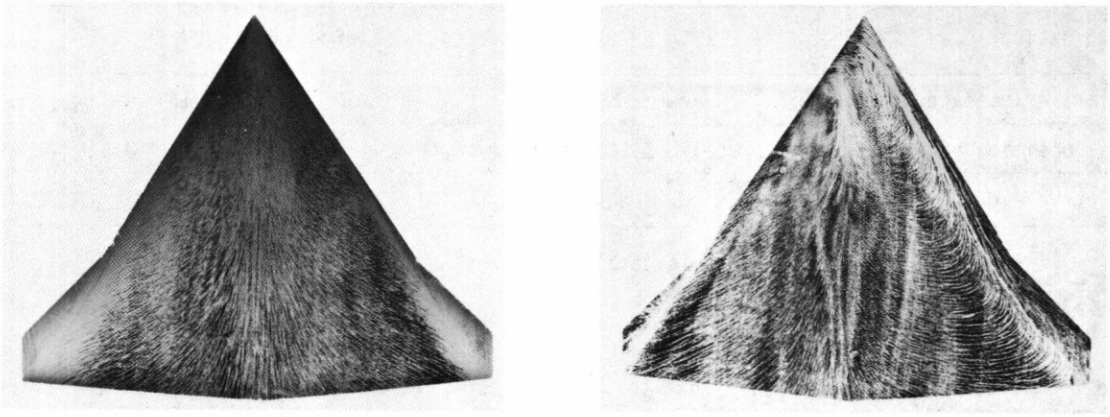

a) $\beta = 0^{o}$ b) $\beta = 5^{o}$

Fig. 4: Flow visualization on configuration 01 at $\alpha = 26.9^{o}$

main part of the upper surface is governed by vortex breakdown. In the corresponding unsymmetrical flow situation an ordinary vortex formation suddenly disappears on the windward side of the wing. According to Fig. 4b the separated flow on the windward side is then of deadwater type and reversed flow is clearly indicated there. On the leeward side of the wing, however the separated flow is still of vortex type with vortex breakdown. From these flow phenomena further additional destabilizing contributions to the rolling moment arise and this leads to the highest lateral instability at $\alpha = 29.6^{o}$.

For even higher angles of attack ($\alpha > 30^{o}$) the reduction of lift in symmetrical flow is accompanied by the disappearance of any vortex formation on both sides of the wing. The separated flow is now of deadwater type everywhere and this situation does not change for unsymmetrical flow ($\beta \neq 0$). This means that the destabilising contributions to the rolling moment, resulting from the upper surface of the configuration, are considerably reduced. On the other hand the lower surface pressure distribution, which becomes more and more important, leads to stabilizing contributions. Therefore lateral stability is recovered for very high angles of attack.

4.2 Effects of wing height

The aerodynamic characteristics of the combinations of the fuselage with the basic wing (1) in low and high position (Configurations L1 and H1) are shown in Fig. 5.

For the high wing configuration H1 the results for symmetrical flow are similar to that for the wing alone up to $\alpha \approx 30^{o}$. In unsymmetrical flow for low angles of attack ($\alpha < 10^{o}$) the typical effects of a high wing position on the lateral stability turn out as well known from attached flow : Due to the crossflow around the fuselage unsymmetrical distributions of local angle of attack and of local lift as functions of wing span occur, which lead to additional stabilizing contributions to the rolling moment. On the windward side of the high wing configuration, for instance, the effective sweep is reduced (planform effect) and the local angle of attack is increased (effect of wing height) as compared to the leeward side, and therefore both stabilizing effects add. In the angle of attack range $10^{o} < \alpha < 30^{o}$ vortex breakdown takes place over the wing and reduces the lift curve slope in symmetrical flow. Due to the addition of the effects of wing planform and wing height in sideslip conditions the asymmetry of vortex breakdown is larger than for the wing alone and the corresponding destabilizing contributions to the rolling moment are more distinctly marked.

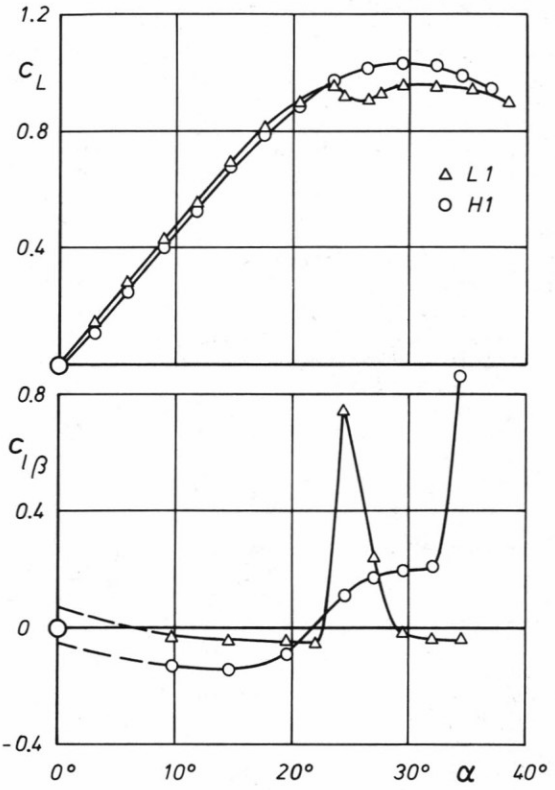

Fig. 5: Aerodynamic characteristics of configurations L1 and H1 (Wing (1), L low wing, H high wing). Effect of wing height.

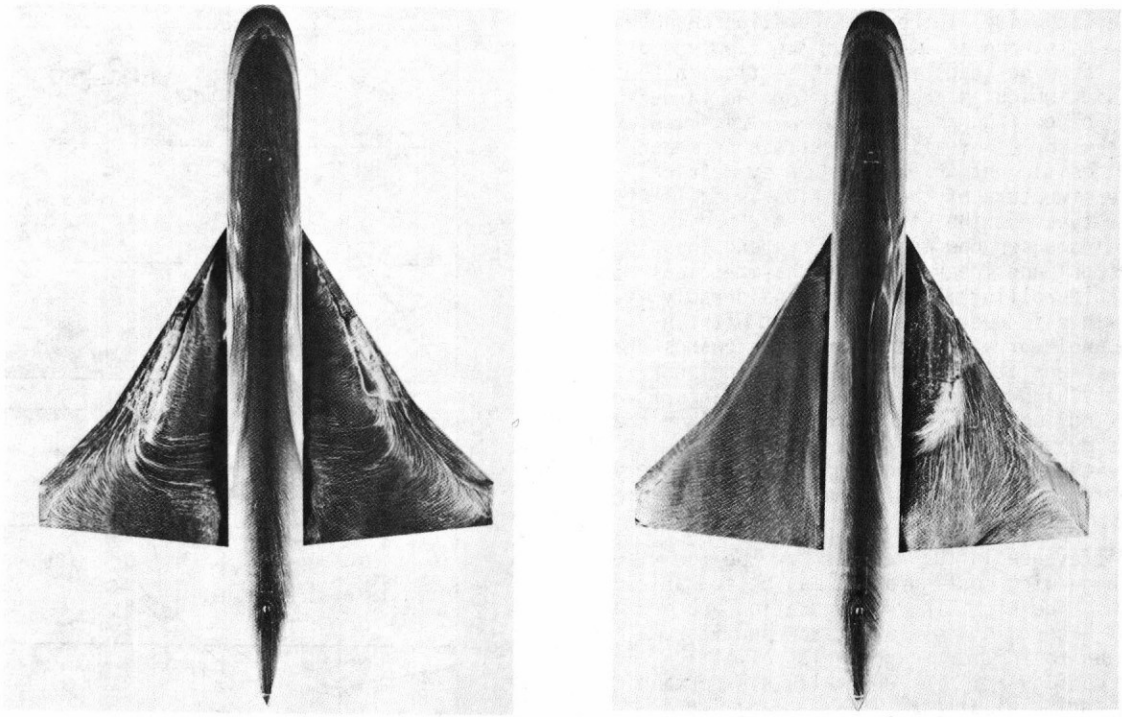

a) $\beta = 0^{o}$ b) $\beta = 5^{o}$

Fig. 6: Flow visualization on configuration L1 at $\alpha = 24.4^{o}$

For $\alpha > 21,5^{o}$ the configuration H1 is unstable. For very high angles of attack ($\alpha > 30^{o}$) flow visualizations in the water-tunnel have shown that there exists a strong effect of the body vortices on the wing flow : The vortices shed from the fuselage are strong enough to influence the flow over the wing. The body vortices join the wing vortices and this leads to a delay in the upstream movement of vortex breakdown over the wing. At very high angles of attack the body vortices are still present and the vortex breakdown point remains fixed to the wing apex. This means in other words that the body vortices enter the deadwater-type flow over the wing and cause some stimulating flow structure there. In symmetrical flow this effect leads to a weaker reduction of lift than for the wing (1) alone according to Fig. 3. In unsymmetrical flow the whole vortex system is easyly shifted to the leeward side in the case of a high wing configuration. This means that the stimulating effect of the body vortices on the structure of the wing flow mainly concentrates on the leeward side. This leads to large destabilizing contributions to the rolling moment and the high wing configuration remains unstable even for very high angles of attack.

The low wing configuration L1 shows a completely different behaviour: At low angles of attack ($\alpha < 10^{o}$) the low wing position leads to destabilizing contributions to the rolling moment. On the windward side of the low wing configuration the effective sweep is reduced (planform effect) but the local angle of attack is decreased (effect of wing height) as compared to the leeward side. Both effects act in opposite direction and therefore the low wing configuration is not so stable as the high wing configuration. For $\alpha > 10^{o}$ vortex breakdown occurs over the wing and reduces the lift curve slope in symmetrical flow. Due to the counteracting effects of planform and wing height, in sideslip conditions the asymmetry of vortex breakdown is weaker than for the high wing configuration and this leads only to a slight destabilizing contribution to the rolling moment. At $\alpha = 23,5^{o}$ a sudden drop of lift is observed in symmetrical flow. At this angle of attack the vortex breakdown point reaches the apex of the wing. An ordinary vortex formation does no longer take place and a deadwater-type separated flow occurs over the wing. In unsymmetrical flow large destabilizing rolling moments are observed and the configuration L1 becomes unstable. The explanation for this behaviour may be taken from Fig. 6. At $\alpha = 24.4^{o}$ in symmetrical flow ($\beta = 0$) the separated flow of deadwater type on the wing is clearly indicated. In unsymmetrical flow ($\beta = 5^{o}$) on the windward side the flow structure is still of deadwater type, but on the leeward side the flow returns to the original state of an ordinary vortex formation near the wing apex and with vortex breakdown somewhere downstream. The occurrence of two different flow structures on both sides of the configuration is due to the fact that for a low wing configuration the fuselage separates both parts of the wing. The sudden change of the flow state on the leeward side of the wing may be governed by the following effects: Due to the low position of the wing in sideslip condition the angle of attack is increased on the leeward side which tends to vortex breakdown and to the formation of a deadwater-type separated flow. On the other hand the angle of sweep of the leading-edge is increased on the leeward side, which tends in the direction of ordinary vortex formation. This planform effect should have been predominant in the present case but it might be that also a stimulating effect from the body vortex

on the leeward side of the configuration has been present. The strong asymmetry of the flow on both sides of the wing leads to higher suction on the leeward side which is the reason for the large instability of configuration L1 at $\alpha = 24.4^{o}$. At even larger angles of attack a certain increase of the lift coefficient is observed in symmetrical flow. The structure of the wing flow is still of deadwater type but the strength of the body vortices increases now more and more and this leads to additional nonlinear lift. In unsymmetrical flow the unstable rolling moments are considerably reduced. This is due to the fact that with increasing angle of attack the tendency towards deadwater-type separation on the leeward side increases and at very high angles of attack the planform effect is no longer able to force the flow on the leeward side to return to the original state. Therefore the instability disappears and for very large angles of attack configuration L1 is stable again.

The difference in the results for the low wing and the high wing configuration may be summarized as follows: The high wing configuration becomes unstable at a certain angle of attack and it remains unstable up to the very high angles of attack. The low wing configuration is unstable in a certain range of angles of attack. This instability is caused by a combination of planform effects and effects of wing height and proper planform modifications might lead to less unstable or even to stable low wing configurations. Therefore the subsequent investigations were mainly concentrated on low wing configurations.

4.3 Effects of strakes

4.3.1 High wing configurations

Some planform modifications by means of a negative strake, wing (2), and a positive strake, wing (3), have also been investigated for high wing positions. The results for the configurations H1, H2 and H3 are plotted in Fig. 7.

The configurations H2 and H3 with strakes show in principle the same behaviour as the clean configuration H1. At low angles of attack the high wing configurations are pretty stable. With increasing angles of attack unsymmetrical vortex breakdown reduces the lateral stability and all configurations become finally unstable at a certain angle of attack.

The negative strake (Configuration H2) causes flow separations of deadwater type which are accompanied on both sides by ordinary vortex formation at the swept part of the leading-edge. At a relatively low angle of attack this configuration reaches its maximum lift coefficient. For even higher angles of attack in symmetrical flow the separated flow over the wing shows a deadwater region which is influenced by the body vortices. In unsymmetrical flow the deadwater structure is maintained on the windward side whereas on the leeward side the deadwater region disappears and the separated flow returnes to the former state with a concentrated vortex near the apex and vortex breakdown somewhere downstream. Both flow states are clearly indicated in Fig. 8a and it is quite obvious that the configuration is unstable due to different types of flow separation on the windward and the leeward side.

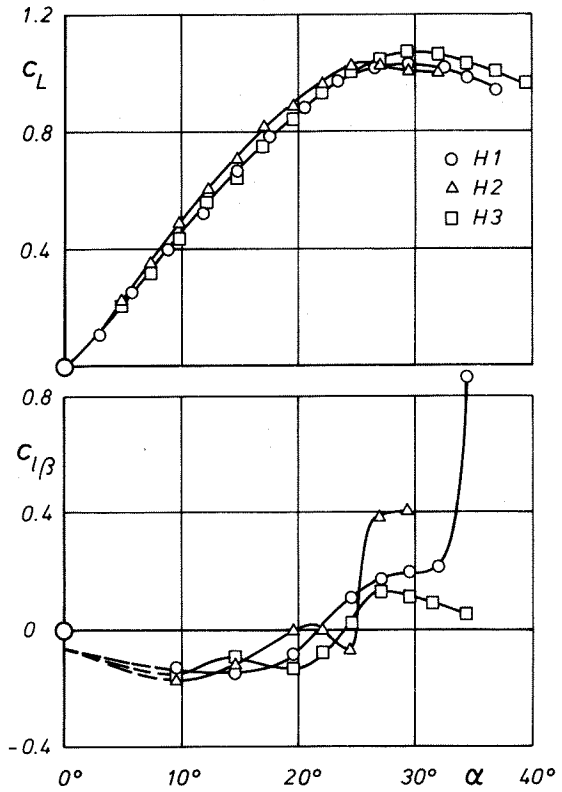

Fig. 7: Aerodynamic characteristics of configurations H1, H2 and H3 (Wings (1), (2), (3) in high wing position). Effects of different strake shapes.

The positive strake (Configuration H3) prevents the occurrence of deadwater regions. Up to very high angles of attack the body vortices and the strake vortex are unified and the flow is governed by vortex breakdown which does not reach the apex of the strake. In unsymmetrical flow the instability is caused by unsymmetrical vortex breakdown, which may be taken from the flow visualization according to Fig. 8b.

4.3.2 Low wing configuration with negative strakes

The aerodynamic characteristics of the combination of the fuselage with the basic wing (1) (Configuration L1) and with two negative strake wings (2) and (7) in low position (Configuration L2 and L7) are shown in Fig. 9.

In symmetrical flow the typical behaviour of low wing configurations turns out. The effect of a negative strake is distinctly marked by a certain shift of the lift drop towards smaller angles of attack. Due to the reduction of the leading-edge sweep close to the fuselage the final upstream movement of the vortex breakdown point is increased and the deadwater type of flow separation occurs already at smaller angles of attack.

In unsymmetrical flow all configurations show the instability in a certain angle of attack range. For configuration L1 it is due to different types of flow separations on the windward and on the lee-

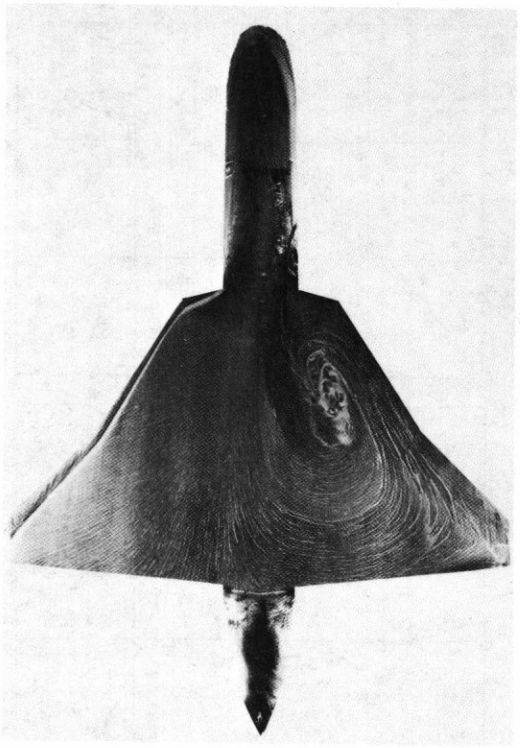

a) Configuration H2

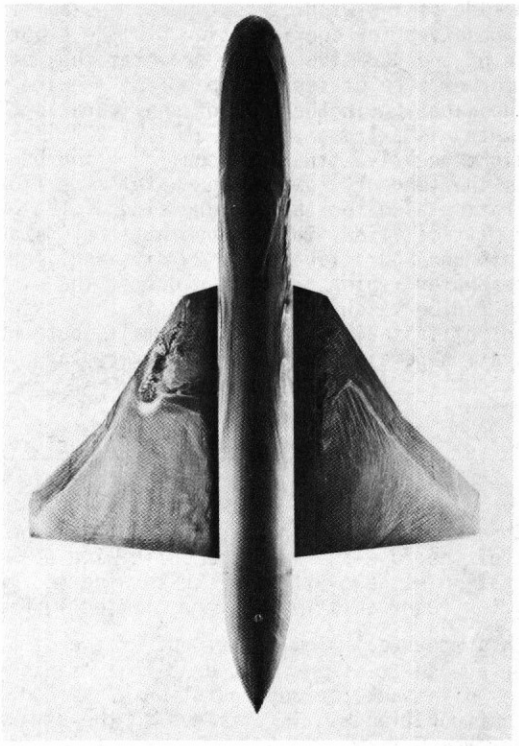

c) Configuration L2

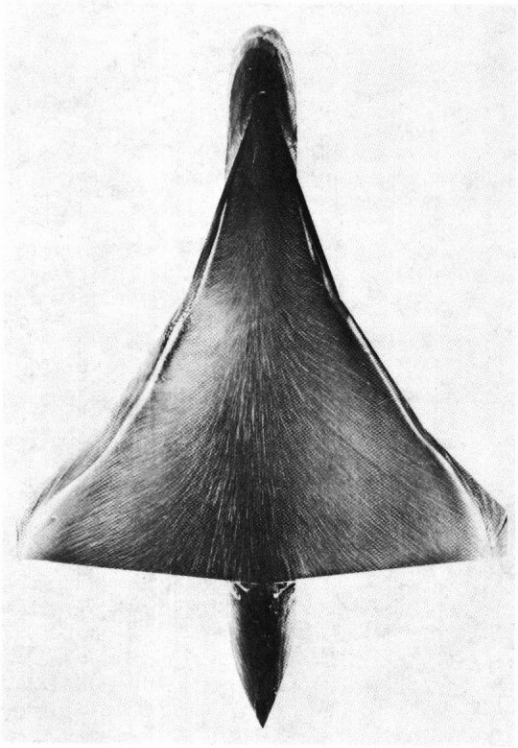

b) Configuration H3

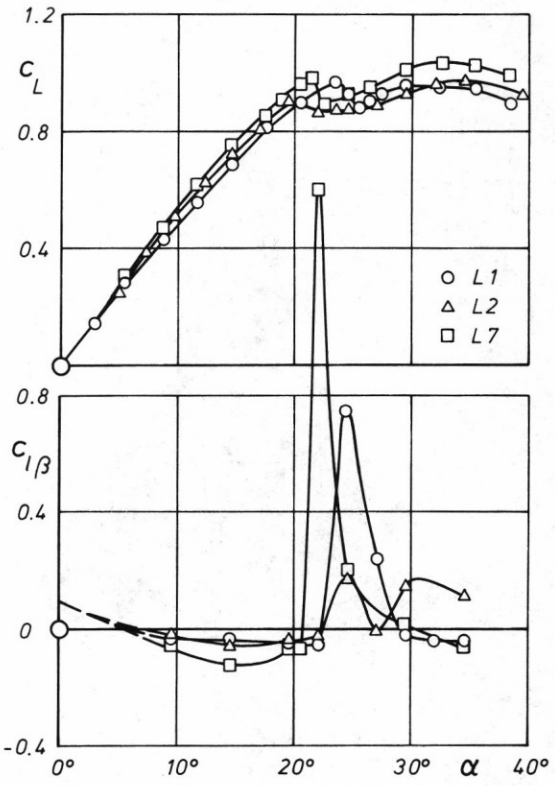

Fig. 8: Flow visualization on configurations H2, H3 and L2 at $\alpha = 27.5^{o}$ and $\beta = 5^{o}$. Different types of flow causing lateral instability.

Fig. 9: Aerodynamic characteristics of configurations L1, L2 and L7 (Wings (1), (2), (7) in low position). Effect of different negative strakes.

ward side of the wing. This type of instability is also observed for configuration L7. The smooth shape of the negative strake promotes the return to the former type of separation on the leeward side of the wing and in the case of configuration L7 the asymmetry is extremely large at $\alpha = 22^{0}$. The straight negative strake of configuration L2 maintains the tendency towards deadwater-type flow separation also for the leeward side of the wing in unsymmetrical flow. This means that the instability of this configuration is due to different formation of deadwater regions on both sides of the wing which can be taken from Fig. 8c. In this case the amount of instability is rather small, but the configuration remains unstable up to very large angles of attack.

4.3.3. Low wing configuration with positive strake

The aerodynamic characteristics of the combination of the fuselage with the basic wing (1) (Configuration L1) and with the strake wing (3) in low position (Configuration L3) are plotted in Fig. 10.

In symmetrical flow the effect of the strake is a certain shift of the lift drop towards higher angles of attack for configuration L3 as compared to configuration L1. This is due to the strake vortex which forms the initial part of the leading-edge vortex and which causes a delay in the upstream movement of the vortex breakdown point. Fig. 11 indicates that on configuration L3 at $\alpha = 26.9^{0}$ an ordinary vortex formation is still present at the strake accompanied by vortex break-

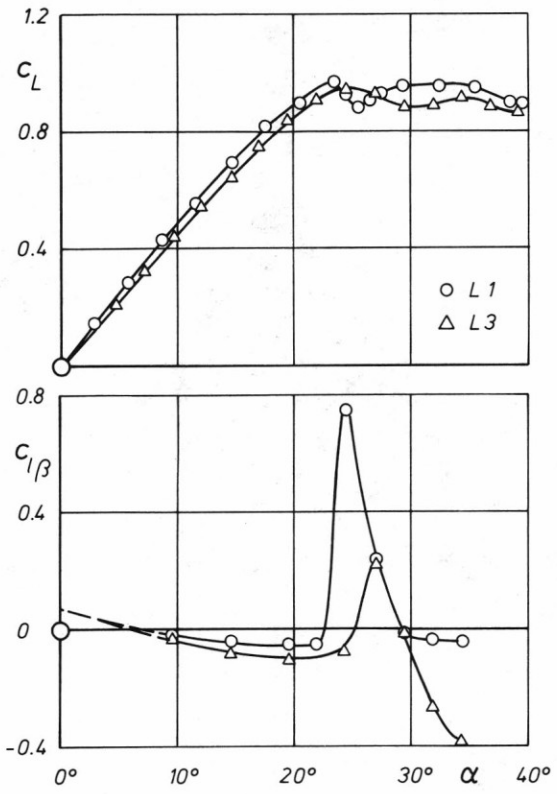

Fig. 10: Aerodynamic characteristics of configurations L1 and L3 (Wings (1), (3) in low position). Effect of a positive strake.

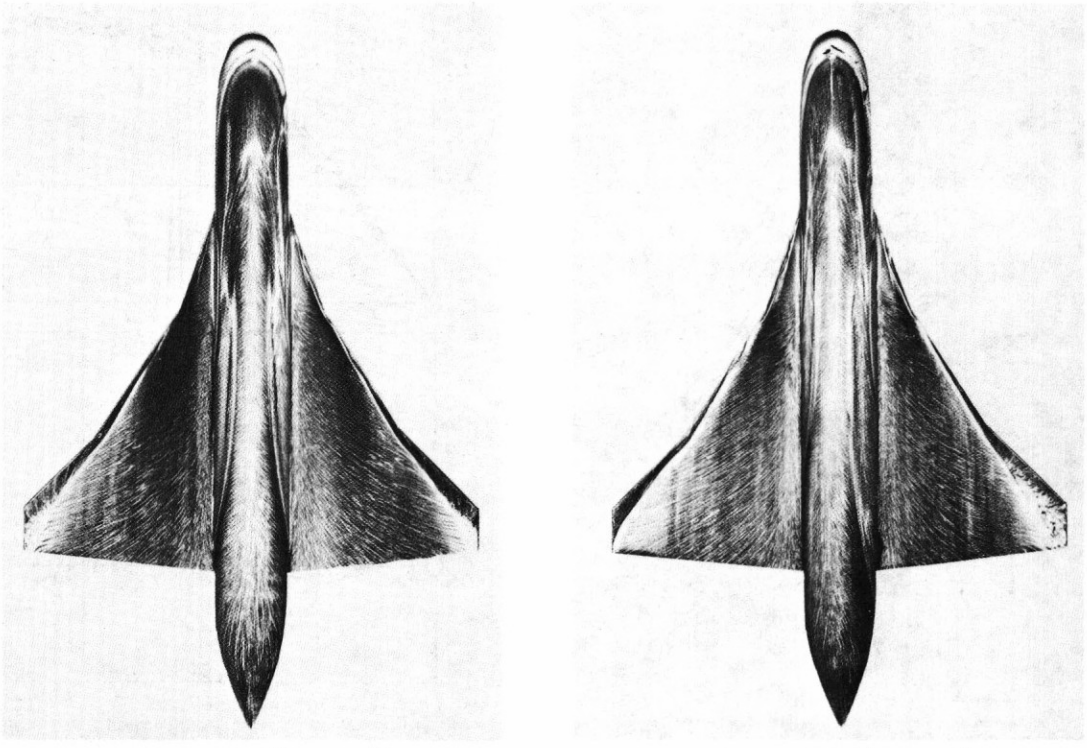

a) $\alpha = 26.9^{0}$, $\beta = 0^{0}$

b) $\alpha = 26.9^{0}$, $\beta = 5^{0}$

Fig. 11: Flow visualization on configuration L3 at $\alpha = 26.9^{0}$ and $\alpha = 34.4^{0}$.

down somewhere downstream. At $\alpha \approx 30^0$ an ordinary vortex formation at the leading-edge disappears and for $\alpha > 30^0$ a deadwater-type separated flow is present on the wing as shown in Fig. 11.

In sideslip conditions unsymmetrical vortex breakdown leads to destabilizing contributions to the rolling moment. In the point of largest instability at $\alpha = 26.9^0$ according to Fig. 11 this flow situation is present. Compared to configuration L1 the strake has changed the flow character which causes instability and correspondingly the amount of instability has been reduced considerably. According to Fig. 11 for $\alpha > 30^0$ a deadwater-type separated flow is present on the windward and on the leeward side of the wing. In this angle of attack range the destabilizing contribution from the upper surface pressure distribution to the rolling moment is reduced, but the stabilizing contribution from the lower surface becomes more and more important. Finally for very large angles of attack the configuration L3 is pretty stable.

4.4 Effects of combined LE and TE modifications

The aerodynamic characteristics of the combination of the fuselage with the wings (4), (5) and (6) in low position (Configurations L4, L5 and L6) are shown in Fig. 12. According to Fig. 2 in this series the kink in the leading- and trailing-edge has been shifted more and more inboard and the angle of sweep of leading- and trailing-edge has also been changed in some parts. The present results have to be compared to those for the configuration L1 according to Fig. 5.

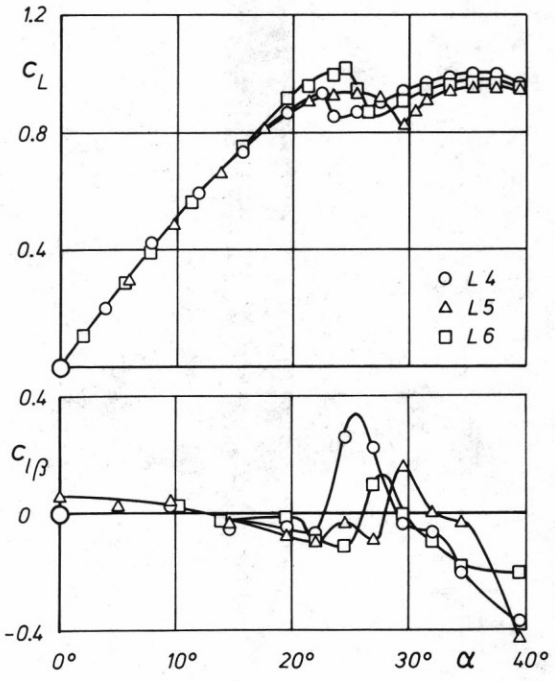

Fig. 12: Aerodynamic characteristics of configurations L4, L5 and L6 (Wings (4), (5), (6) in low position). Effect of different LE and TE modifications.

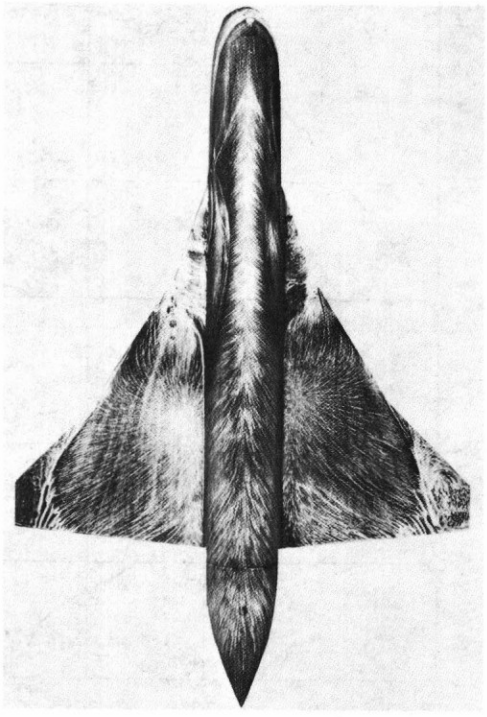

c) $\alpha = 34.4^0$, $\beta = 0^0$

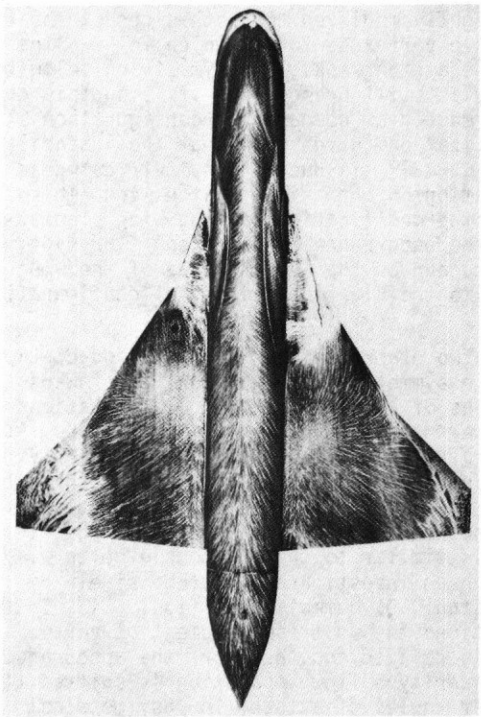

d) $\alpha = 34.4^0$, $\beta = 5^0$

Fig. 11: (continued).

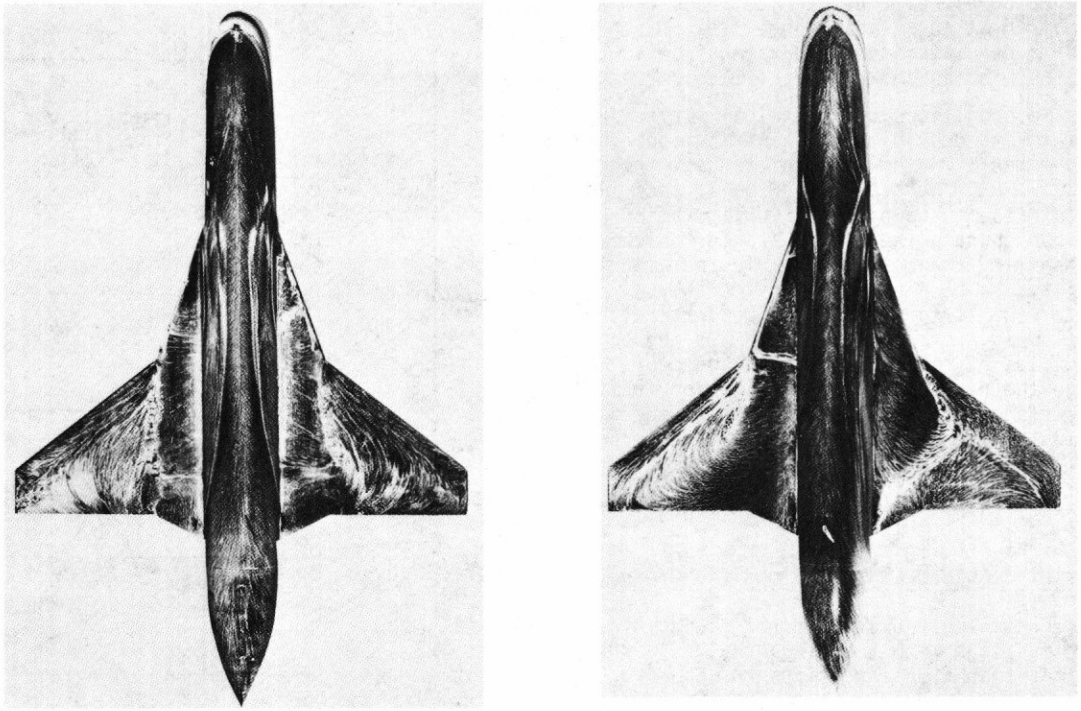

a) $\beta = 0^{o}$ b) $\beta = 5^{o}$

Fig. 13: Flow visualization on configuration L5 at $\alpha = 29.6^{o}$

In symmetrical flow the configuration L4 behaves similar to configuration L1 since the leading-edge is only slightly modified. On both sides of the wing a single vortex is formed which follows the leading-edge at the kink. In unsymmetrical flow the instability is still present but its amount is considerably reduced as compared to configuration L1. Flow visualizations have shown that the instability for $23^{o} < \alpha < 29^{o}$ is due to unsymmetrical deadwater formation on both sides of the wing. This means that the modifications of the wing planform prevented the occurrence of different flow types on the windward and on the leeward side of the wing which led to the high instability of configuration L1.

For the two other configurations L5 and L6 the lift drop in symmetrical flow is shifted towards higher angles of attack. For both configurations the inner part of the wing acts like a strake. At low angles of attack the corresponding strake vortex is separate from the vortex shed from the outer portion of the wing. At higher angles of attack both vortices on each side of the wing merge. This behaviour is similar to that of double delta wings which have been investigated comprehensively by U. Brennenstuhl, D. Hummel [12], [13], [14]. In the joined vortices the upstream movement of vortex breakdown is delayed and therefore the appearance of a deadwater-type flow separation is shifted towards higher angles of attack. In unsymmetrical flow for the configurations L5 and L6 some unstable rolling moments turn out which are again due to unsymmetrical deadwater formation. As a typical example for this flow situation Fig. 13 shows the flow visualization for configuration L5 at

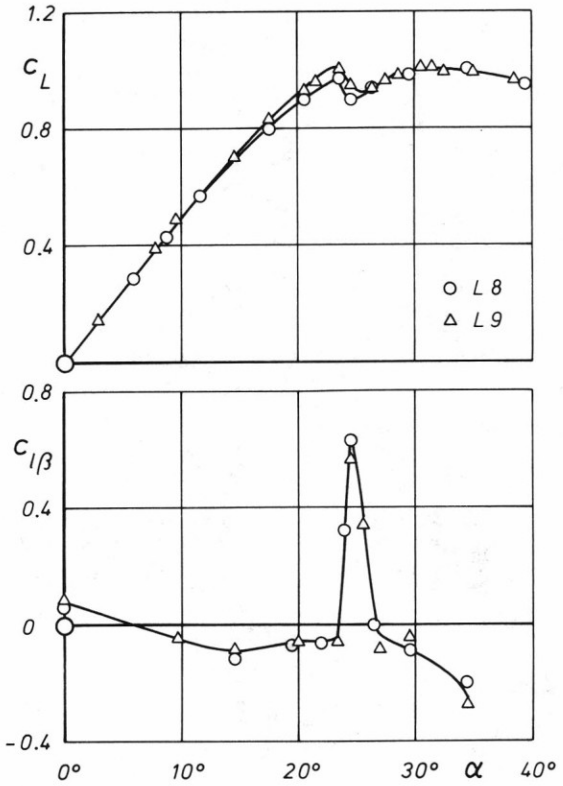

Fig. 14: Aerodynamic characteristics of configurations L8 and L9 (Wings (8), (9) in low position). Effect of TE shape.

$\alpha = 29{,}6^{0}$. The amount of instability is for both configurations L5 and L6 relatively small and at very high angles of attack lateral stability is re-established due to the decreasing influence from the upper surface and the increasing effect from the lower surface of the wing.

4.5 Effects of TE modifications

The aerodynamic characteristics of the combination of the fuselage with the wings (8) and (9) in low position (Configurations L8 and L9) are shown in Fig. 14 for the sake of completeness. The results for both configurations are practically identical and they differ only slightly from those for the configurations L4 and L1 according to Figs. 12 and 5. The leading-edge shape is responsible for the vortex formation and this shape has been kept constant for the configurations L1, L8 and L9. Modifications of the trailing-edge shape do not alter the results significantly.

4.6 Trigger effects

During the experimental program some trigger devices have been used to influence the flow in such a way that lateral stability is achieved for the whole angle of attack range.

One type of trigger devices were vortex generators in the form of small triangular winglets placed perpendicular to the wing surface at the leading-edge of both sides of the wing. Devices of this kind have been successfully applied for other configurations by D. Welte, S. Ehekircher [9]. For the present configuration L1 some improvements were possible by the application of these devices, but lateral stability within the whole angle of attack range was not obtainable.

Another type of trigger devices were small chines in the form of ledges or fences placed parallel to the body axis on both sides of the fuselage. These body fences were originally aimed to fix the separation of the body vortices. Later it turned out that such fences might have favourable effects on the lateral stability, and then some explorative variations of the arrangement of the fences have been tested.

One of these few configurations is shown in Fig. 15. The wing-body combination with the positive strake wing in low position (Configuration L3) has been modified by body fences (Configuration L3F). These fences were manufactured from a thin aluminium sheet. The relative height was $h/R = 0.125$ and the relative length was $l/L = 0.27 \approx c_R/2$. These fences were fixed to the fuselage at $\varphi = 80^{0}$ and the front end of the fence was located at the tip of the root chord c_R of the wing-body-combination.

The aerodynamic characteristics of this wing-body-combination (Configuration L3F) are shown in Fig. 16 and compared to the results of the confi-

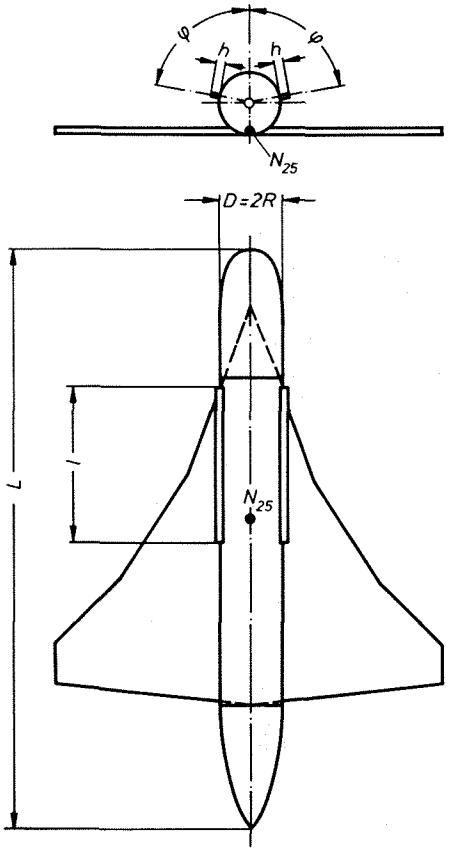

Fig. 15: Body fences on configuration L3F (Wing (3) in low position, fuselage with fences)

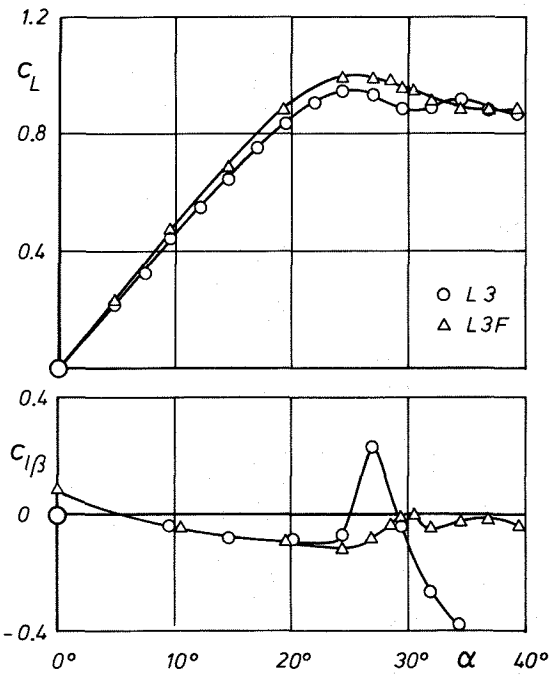

Fig. 16: Aerodynamic characteristics of configurations L3 and L3F (Wing (3) in low position, body without and with fences). Trigger effect of body fences.

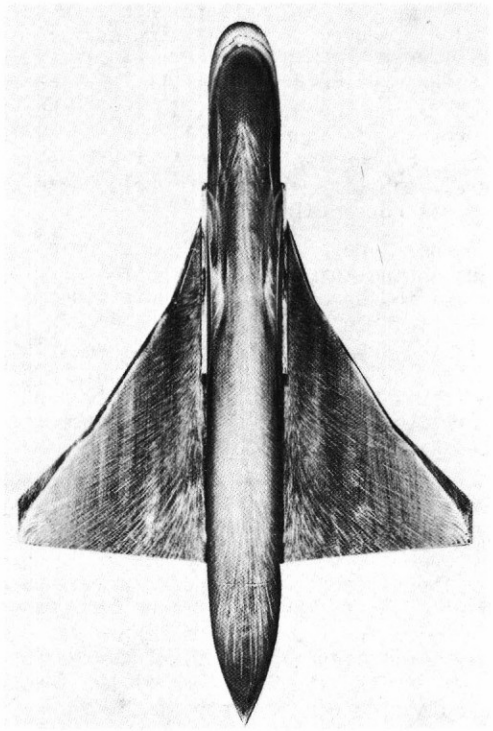

a) $\alpha = 26.9^{o}$, $\beta = 0^{o}$

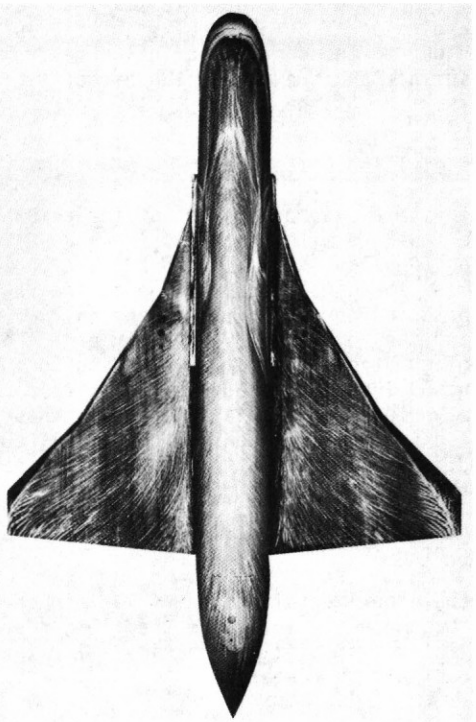

b) $\alpha = 26.9^{o}$, $\beta = 2.5^{o}$

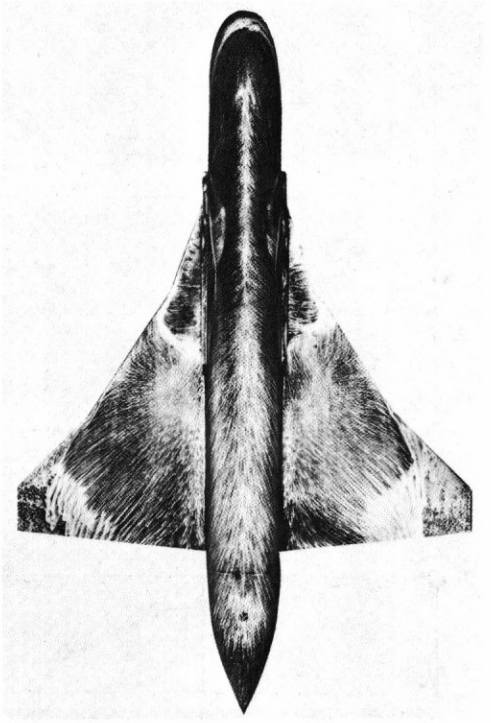

c) $\alpha = 34.4^{o}$, $\beta = 0^{o}$

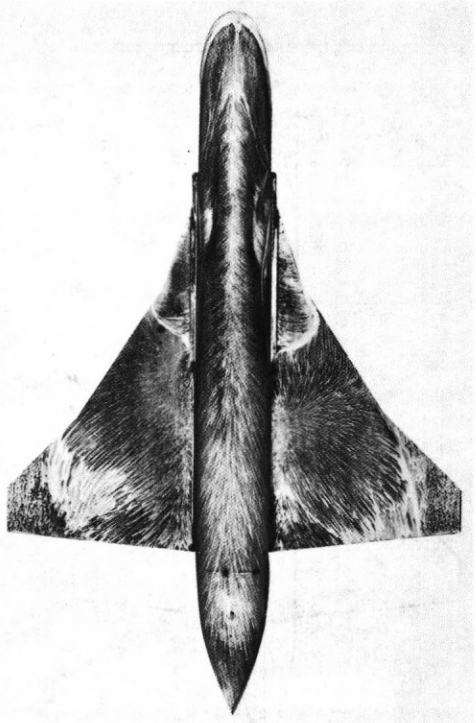

d) $\alpha = 34.4^{o}$, $\beta = 2.5^{o}$

Fig. 17: Flow visualization on configuration L3F at $\alpha = 26.9^{o}$ and $\alpha = 34.4^{o}$.

guration L3 without body fences. In symmetrical flow the fences lead to a distinctly higher maximum lift coefficient and for angles of attack $\alpha > \alpha_{c_{L\,max}}$ a slight decrease of the lift coefficient is observed. For very high angles of attack ($35^0 < \alpha < 40^0$) the lift coefficient remains constant and no second maximum is observed for the lift coefficient.

Results of the flow visualization on configuration L3F are given in Fig. 17. They have to be compared to Fig. 11 which shows the results of flow visualizations on configuration L3 for the same angles of attack.

At $\alpha = 26.9^0$ in symmetrical flow vortex breakdown occurs over the wing and the vortex breakdown point is located somewhere over the strake. A comparison between Fig. 17 and Fig. 11 for symmetrical flow at $\alpha = 26.9^0$ shows the same type of flow over the wing without and with body fence. From the slope of the secondary separation line on the strake one might deduce a slight difference in vortex breakdown position: The fence shifts the breakdown point a little bit downstream, but this feature is not distinctly marked, although it would explain the higher lift coefficients for the configuration L3F with fences. The main effect of the body fences in symmetrical flow can be observed for $\alpha = 26.9^0$ on the fuselage: Without the fences (Fig. 11) the body vortices lie over the fuselage. They move slightly outboard and over the rear part of the wing some interference with the wing flow takes place. With the fences (Fig. 17) the body vortices lie closer to the fuselage. Already in the rear part of the fences they move outboard under the influence of the wing vortex, and merge with the wing flow. This indicates a stronger interference of the body vortices with the wing flow in symmetrical free stream conditions. This interference causes a delay in the vortex breakdown upstream movement which leads to slightly higher lift coefficients.

At very high angles of attack vortex breakdown reaches the apex of the strake. An ordinary vortex formation does no longer take place and a deadwater-type flow separation is observed over the wing. Without the body fences (Configuration L3) at these angles of attack the body vortices are for the first time influenced by the wing flow. According to Fig. 17 the body vortices merge with the deadwater region of the wing. They increase the suction level there which leads to the augmentation of lift which can be seen from Fig. 16. For the wing-body-combination with the body fences (Configuration L3F) the interference of the body vortices with the wing flow has been established by the fences even at lower angles of attack and in the high angles of attack range no new effect is observed. Fig. 17 shows the interference of the body vortices with the wing flow which starts already in the rear part of the fence. The establishment of a deadwater-type flow separation leads to a slight reduction of lift according to Fig. 16, but since no new effect occurs no further increase of lift can be observed. This means in other words that the body fences favour the interference between body vortices and wing flow even at low angles of attack and thus the lift increase, which is observed for the configuration L3 without the body fences at very high angles of attack, is shifted towards lower angles of attack for the configuration L3F with fences.

The most interesting results turn out for unsymmetrical flow. Fig. 16 shows that the configuration L3F with body fences is stable in the whole angle of attack range. To explain this behaviour results of flow visualization for the wing-body-combination with body fences (Configuration L3F) are given in Fig. 17 for $\alpha = 26.9^0$ and $\alpha = 34.4^0$. For these angles of attack the largest differences exist between the c_{l_β}-derivatives of the configurations L3 and L3F. The corresponding flow visualizations for the wing-body-combination without body fences (Configuration L3) may be taken from Fig. 11.

The instability of configuration L3 is caused by unsymmetrical vortex breakdown. Fig. 11 shows for $\alpha = 26.9^0$ and $\beta = 2.5^0$ that on the windward side there exists practically no effect of the body vortex on the wing flow, but on the leeward side the effect of the body vortex is distinctly marked and this leads to the unstable rolling moments. For the wing-body-combination with the body fences (Configuration L3F) Fig. 17 indicates that an interference of the body vortices with the wing flow takes place on both sides of the configuration. On the leeward side the unfavourable situation is the same as for the configuration L3 without the body fences, but on the windward side the body fences cause a favourable interference effect. Thus the asymmetry of the flow is reduced and the configuration is stable.

At very high angles of attack the configuration L3F with the body fences remains stable but the amount of stability is considerably reduced as compared to configuration L3 without the body fences. For both configurations a deadwater-type flow separation is present over the wing and in unsymmetrical flow the deadwater structure is different on both sides of the wing. The body fences influence the structure of the deadwater flow. A comparison of Figs. 11 and 17 for $\alpha = 34.4^0$, $\beta = 2.5^0$ indicates that the body fences might hinder the interference between the body vortices and the wing flow, especially on the windward side. This could explain the reduction of lateral stability by the body fences at very high angles of attack.

From this discussion it may be concluded that on the one hand it was possible to find a configuration by simple means, which shows lateral stability for the whole angle of attack range, but on the other hand this configuration is not at all optimized. The behaviour of configuration L3F at very high angles of attack suggests for instance to shorten the body fences at the rear end for further improvement of the aerodynamic characteristics. Investigations of this kind have not yet been performed but they should be carried out in order to find those configurations which lead to a maximum improvement of the aerodynamic characteristics by a minimum of geometric modifications.

5. Summary

The lateral stability characteristics of a series of wing-body-combinations has been investigated at the Institut für Strömungsmechanik of Technische Universität Braunschweig. The configurations were composed of a fuselage of length/diameter ratio $L/D = 9.25$ and 9 different wings of aspect ratios $2.14 \leq A \leq 2.64$ in high and low position. In addition some configurations were equipped by small body fences in order to influence

the flow field and to trigger the aerodynamic characteristics. Six-component balance measurements have been carried out in the 1.3 m low-speed wind-tunnel up to high angles of attack and additional flow visualizations have been performed in the wind-tunnel as well as in the water-tunnel of the institute.

In symmetrical flow for all configurations vortex breakdown over the wing leads to a reduction in lift curve slope and a sudden loss of lift is observed when the wing vortices are completely destroyed by vortex breakdown and a deadwater-type flow is established over the wing. In unsymmetrical flow unstable rolling moments occur in that angle of attack range in which the sudden lift loss is observed in symmetrical flow. At low angles of attack, for which attached flow or ordinary leading-edge vortex flow without vortex breakdown is present, the wing planform effect (reduction of sweep on the windward side and increase of sweep on the leeward side) leads to stabilizing contributions to the rolling moment. A low wing arrangement has destabilizing effects and a high wing arrangement leads to stabilizing effects on the rolling moment due to the induced angle of attack distribution in unsymmetrical flow.

At higher angles of attack for which vortex breakdown occurs over the wing these effects change: Unsymmetrical vortex breakdown due to the planform effects reduces the lateral stability. A low wing arrangement leads to stabilizing contributions to the rolling moment since the angle of attack distribution in unsymmetrical flow reduces the asymmetry of vortex breakdown. Correspondingly high wing arrangements cause destabilizing contributions to the rolling moment.

For low wing arrangements the flow on both sides of the wing is divided by the fuselage. The distance between the body vortices and the wing vortices is relatively large and therefore interference effects are weak. For high wing arrangements both sides of the wing influence each other. The body vortices occur at the same level as the wing vortices. The corresponding interference effects are large and therefore high wing arrangements are much more unstable than low wing arrangements.

Unstable rolling moments were finally caused by different flow situations

(i) Unsymmetrical vortex breakdown, which led to relatively weak instability

(ii) Unsymmetrical formation of the deadwater region over the wing which led also to relatively weak instability

(iii) Deadwater-type flow on the windward side and vortex flow with vortex breakdown on the leeward side of the wing. In this case the instability was extremely large.

By small modifications of the fuselage contour in form of body fences it is possible to trigger the flow in such a way that lateral stability is achieved for the whole angle of attack range. The basic configuration for the application of such devices should be only slightly unstable. The stabilizing effect of the body fences has been found to be a favourable interference effect between the body vortices and the wing flow on the windward side of the configuration.

6. References

[1] D. Hummel: Zur Umströmung scharfkantiger schlanker Deltaflügel bei großen Anstellwinkeln.
Z. Flugwiss. 15 (1967), 376-385.

[2] D. Hummel, G. Redeker: Über den Einfluß des Aufplatzens der Wirbel auf die aerodynamischen Beiwerte von Deltaflügeln mit kleinem Seitenverhältnis beim Schiebeflug.
Jb. 1967 der WGLR, 232-240.

[3] W. Kraus, H. John: Aerodynamische Eigenschaften von Kampfflugzeugen bei hohen Anstellwinkeln.
DGLR-Vortrag Nr. 78-113 (1978).

[4] H. John, W. Kraus: High angle of attack characteristics of different fighter configurations.
AGARD-CP 247 (1978), 2-1 to 2-15.

[5] W. Staudacher, B. Laschka, Ph. Poisson-Quinton, J.P. Ledy: Aerodynamic characteristics of a fighter-type configuration during and beyond stall.
AGARD-CP 247 (1978), 8-1 to 8-15.

[6] C.W. Smith, C.A. Anderson: Design guidelines for the application of forebody and nose strakes to a fighter aircraft based on F-16 wind tunnel testing experience.
AGARD-CP 247 (1978), 5-1 to 5-11.

[7] J.E. Lamar, J.M. Luckring: Recent theoretical developments and experimental studies pertinent to vortex flow aerodynamics - with a view towards design.
AGARD-CP 247 (1978), 24-1 to 24-31.

[8] A.M. Skow, A. Titiriga, W.A. Moore: Forebody/wing vortex interactions and their influence on departure and spin resistance.
AGARD-CP 247 (1978), 6-1 to 6-26.

[9] D. Welte, S. Ehekircher: Wind tunnel measurements and analysis of some unusual control surfaces on two swept wing fighter configurations.
AGARD-CP 265 (1979), 6-1 to 6-10.

[10] W. Kraus: Delta canard configuration at high angle of attack.
Z. Flugwiss. Weltraumforsch. 7 (1983), 41-46.

[11] W. Staudacher: Vorderkanten-Klappensysteme für schlanke Flügel: "Vortex Flaps"?
DGLR-Vortrag Nr. 82-103 (1982).

[12] U. Brennenstuhl, D. Hummel: Untersuchungen über die Wirbelbildung an Flügeln mit geknickten Vorderkanten.
Z. Flugwiss. Weltraumforsch. 5 (1981), 375-381.

[13] U. Brennenstuhl, D. Hummel: Weitere Untersuchungen über die Wirbelbildung an Flügeln mit geknickten Vorderkanten.
Z. Flugwiss. Weltraumforsch. 6 (1982), 239-247.

[14] U. Brennenstuhl, D. Hummel: Vortex formation over double-delta wings.
ICAS Proceedings 1982, 1133-1146.